

# A Zero-Added-Loss Multiplexing (ZALM) Source Simulation

Jerry Horgan<sup>†</sup>, Alexander Nico-Katz<sup>‡</sup>, Shelbi L. Jenkins<sup>§</sup>, Ashley N. Tittelbaugh<sup>§</sup>, Vivek Vasan<sup>†</sup>, Rohan Bali<sup>§</sup>, Marco Ruffini<sup>†</sup>, Boulat A. Bash<sup>§</sup>, and Daniel C. Kilper<sup>†</sup>

**Abstract**—Zero-Added-Loss Multiplexing (ZALM) offers broadband, per-channel-heralded EPR pairs, with a rich parameter space that allows its performance to be tailored for specific applications. We present a modular ZALM simulator that demonstrates how design choices affect output rate and fidelity. Built in NetSquid with QSI controllers, it exposes 20+ tunable parameters, supports 'IDEAL' and 'REALISTIC' modes, and provides reusable components for Spontaneous Parametric Down Conversio (SPDC) sources, interference, Dense Wavelength Division Multiplexing (DWDM) filtering, fiber delay, active polarization gates, detectors, and lossy fiber. Physics-based models capture Hong–Ou–Mandel (HOM) visibility, insertion loss, detector efficiency, gate errors, and attenuation. Using this tool, we map trade-offs among fidelity, link distance, and entangled pairs per use, and show how SPDC bandwidth and DWDM grid spacing steer performance. Using the default configuration settings, average fidelity remains constant at  $\sim 0.8$  but the ebit rate decreases from  $\sim 0.0175$  at the source to 0.0 at 50 km; narrowing the SPDC degeneracy bandwidth increases the ebit rate significantly without affecting fidelity. The simulator enables co-design of source, filtering, and feed-forward settings for specific quantum memories and integrates as a building block for end-to-end quantum-network studies.

## I. INTRODUCTION

Robust entanglement distribution is a foundational requirement for the future quantum internet, as laid out by Kimble [1] and Wehner et al. [2]. While much research has focused on optimising the rate and fidelity of this entanglement distribution, the next step is integrating with quantum memories to form functional quantum memory networks. Adopting the principles of systems engineering, we argue that a holistic, end-to-end analysis of the network architecture is critical. This perspective integrates the performance of quantum entanglement sources, the fidelity degradation across quantum channels, and the efficiencies of quantum memories. To address this, we model a novel quantum source specifically engineered for high-efficiency loading into quantum memories, thereby improving the performance of the entire quantum network. Quantum entanglement sources come in many forms, with different natural wavelengths, emission efficiencies, and bandwidths, as described by Eisaman et al. [3]. Placing these sources into

two main categories, we can look at their emission properties as either deterministic, such as the very precise wavelengths emitted by quantum dots, or probabilistic, whereby the output photons will be found within a specific bandwidth centred at a known wavelength. Although deterministic sources simplify network setups, the broadband capabilities of probabilistic sources allow for greater use of the available spectrum and enable the use of common classical network management techniques, such as routing and spectrum allocation, see Bali et al. [4]. To scale quantum networks beyond simple point-to-point links, quantum memories are an essential component. They provide the crucial capability to synchronise operations between distant nodes and to mitigate the inherently probabilistic nature of entanglement generation and swapping protocols. As such, memories form the cornerstone of quantum repeater architectures. The search for a practical physical implementation has led to significant research in solid-state systems. For instance, Weber et al. [5] showed that defects, or vacancies, in diamond are a practical and robust mechanism to provide room-temperature quantum memories. Further work by Braded et al. [6] highlighted the attributes of the other group IV elemental defects in diamond, with Silicon showing considerable coherence times,  $> 1$ s, and a more efficient spin-photon interface. However, successfully interfacing with these memories is a significant challenge, with Bersin et al. [7] and Raymer et al. [8] detailing the specific requirements on the incoming photons' properties, such as bandwidth and wavelength matching. The Zero-Added-Loss Multiplexing (ZALM) protocol introduced by Chen et al. [9] provides for a broadband source with high memory loading efficiency. As there is currently no agreed implementation of the transmitter (Tx) component of this protocol and there are numerous configuration options of each of the transmitter subcomponents, we created a configurable simulation to determine the optimal transmitter architecture for maximising entanglement distribution rates and fidelity.

## II. THE ZALM SOURCE

ZALM, as described by Chen et al. [9] and Shapiro et al. [10], is a broadband, deterministic source-in-the-middle architecture that is optimised for memory loading through the spin-photon interface. ZALM combines a pair of probabilistic SPDC sources into a deterministic quantum entanglement source where the timing and wavelength of a quantum entanglement pair emission is known by the source and communicated to the receiver in advance of transmission. This information is used by the receiving node to efficiently convert the incoming photons for maximum compatibility with the

This work is supported by the Science Foundation Ireland grants 20/US/3708, 21/US-C2C/3750, and 13/RC/2077 P2 and National Science Foundation under Grant No. CNS-2107265.

<sup>†</sup>J. Horgan, V. Vasan, M. Ruffini, and D. Kilper are with CONNECT Centre, Trinity College Dublin, Dublin, Ireland (e-mail: horganj3@tcd.ie; vasanv@tcd.ie; marco.ruffini@tcd.ie; dan.kilper@tcd.ie).

<sup>‡</sup>A. Nico-Katz is with Trinity Quantum Alliance, Trinity College Dublin, Dublin, Ireland (e-mail: nicokata@tcd.ie; ).

<sup>§</sup>S. L. Jenkins, A. N. Tittelbaugh, and B. A. Bash is with the Electrical and Computer Engineering Department, University of Arizona, Tucson, AZ, USA (e-mail: boulat@arizona.edu).

memory loading process, hence there is Zero-Added-Loss at the quantum receiver. Whilst the emission rate of the ZALM source may be lower than other quantum entanglement sources, it has the advantage of only emitting entangled pairs that are capable of being loaded into a memory at the receiver. It classically heralds the receivers to expect a photon within a certain time frame allowing the unheralded (non entangled) photons to be discarded.

each detector has an associated central wavelength for the idler photon with a margin of error  $< \pm 50\%$  of the DWDM channel width. The coincidence counts at the detectors are then heralded at the (vii) heralding station, which notifies the (viii) post-processor any corrections to be applied to the signal photons.

Knowing the central wavelength of the idlers, the approximate wavelength of the signal photons can be determined based on the principles of energy conservation used by the SPDC processes. Therefore, the smaller the DWDM channel bandwidth, the more accurate this approximation will be, improving the memory loading efficiency in the receiving node. This is the key feature of the ZALM source, and is what makes it a deterministic source.

The steps / components listed here are explained in greater detail in the following section.

### III. THE ZALM SOURCE MODEL

The ZALM source produces entanglement in multiple stages. Initially, entanglement is generated using SPDC processes, where a crystal is placed in a sagnac configuration, see Fig. 2. Two SPDC processes are used in the ZALM source and each creates, with some level of probability, a two-qubit quantum entangled state. These separate quantum states are then entangled, again with some level of probability, with each other to create a four-qubit state. These stages are now described in more detail.

#### A. Spontaneous Parametric Down Conversion

There are three types of SPDC process; 0, I, and II. Each SPDC process is pumped by a laser, but the conservation of energy in each process type acts differently, which can affect the wavelength, emission angle, polarisation, and the bandwidth of the emitted photons.

A type-0 SPDC process emits two photons with the same polarisation as the pump laser, creating a  $|\Phi\rangle$  Bell state. Type-I SPDC processes emit photons at different angles. The emitted photons are both co-polarised, but they are orthogonal to the pump laser polarisation, again creating a  $|\Phi\rangle$  Bell state. However, type-I processes are less efficient than type-0 and therefore are not used in the model. Type-II SPDC processes emit orthogonally polarised photons, and therefore emit a  $|\Psi\rangle$  Bell state. Note, that the wavelengths of each photon will be symmetric around the central wavelength,  $\lambda$ .

A degenerate SPDC process will create two photons, each with exactly half of the pump photon's energy, and will therefore be at the same wavelength. This is similar to a narrowband source and not desired in the ZALM source configuration. However, a non-degenerate SPDC process will unevenly distribute the pump photon's energy resulting in the signal and idler photons having different wavelengths. These wavelengths typically follow a Gaussian distribution across a known range and provide for a broadband source.

1) *Signal-Idler separation:* The model allows for two distinct mechanisms to separate the signal and idler photons.

- 1) A polarising beam splitter can be configured to always have the H polarised photon be the signal and the V

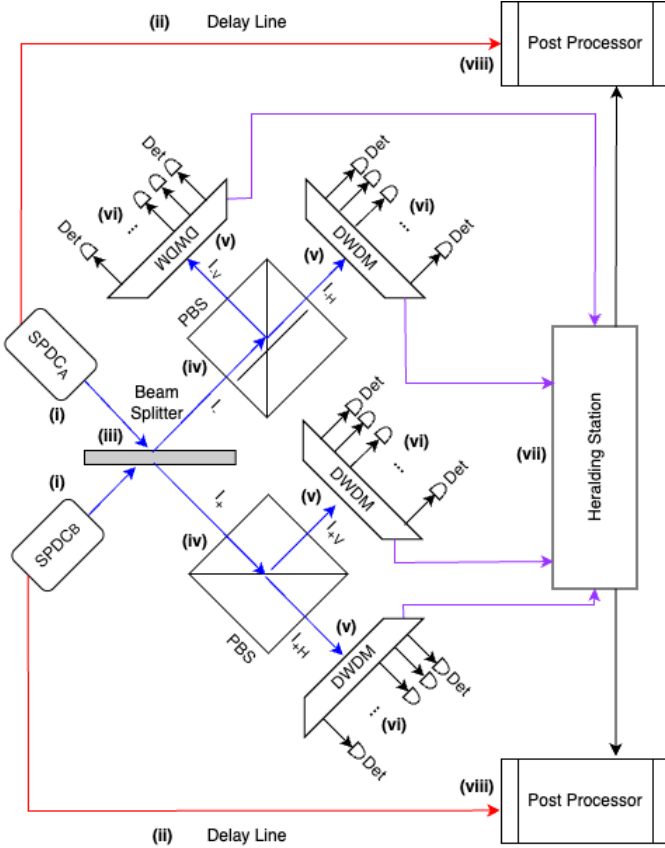


Fig. 1: ZALM source components.

The ZALM source consists of (i) two SPDC processes which are triggered simultaneously. These SPDC processes are configured to each produce a two-qubit entangled state. The qubits are physically photons<sup>1</sup> that are polarization encoded. The photons produced by each SPDC process are labelled as signal and idler. The signal photons go directly to (ii) a delay line for later processing, whilst the idler photons are passed through (iii) a beam splitter (BS).

The beam splitter, with some probability, will entangle the two idler photons, producing a four-qubit quantum state (which includes the two signal photons in the delay lines). The two idler photons are then emitted from the beam splitter where they pass through (iv) a polarising beam splitter (PBS), which separates them into their respective states. The PBSs are connected to (v) DWDM filters, each of which have as many (vi) detectors attached as channels available. Therefore,

<sup>1</sup>The terms Photons and Qubits are used interchangeably in the text. When discussing a photon, the authors generally discuss the physical properties associated with the photon and not the quantum state. When qubits are used, the authors focus on the quantum state of the system.

polarised photon be the idler, or vice versa. When the two SPDC processes are configured inversely to each other, i.e. with orthogonally polarised idlers, a  $|\Psi\rangle$  state will always be produced.

- 2) A Dichroic Mirror (DM) will separate photons based on a selected wavelength, which will either transmit or reflect the photon, see Fig. 2.

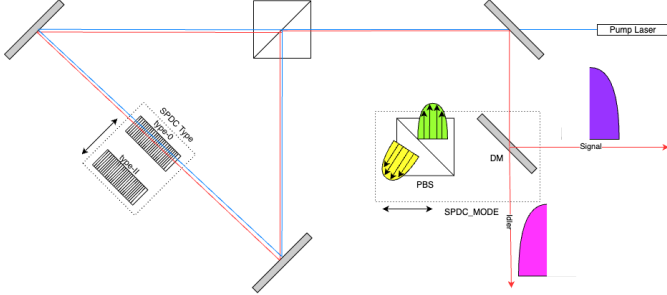


Fig. 2: SPDC configuration options.

### B. Four-Qubit State Generation

In the ZALM source, a 50:50 beam splitter is used to create entanglement between the two 2-qubit states, resulting in a four-qubit state. Whilst the Bell state generated at each SPDC process could be any of the four possible, it may not be known which encoded photon is the idler or the signal. Therefore, any combination of the four Bell states,  $|\Phi\rangle_+$ ,  $|\Psi\rangle_+$ ,  $|\Psi\rangle_-$ , or  $|\Phi\rangle_-$  can be created at the beam splitter.

$$\begin{aligned}
 |\Phi\rangle_+ &= \frac{1}{\sqrt{2}}(|00\rangle + |11\rangle) = \frac{1}{\sqrt{2}}(|HH\rangle + |VV\rangle) \\
 |\Psi\rangle_+ &= \frac{1}{\sqrt{2}}(|01\rangle + |10\rangle) = \frac{1}{\sqrt{2}}(|HV\rangle + |VH\rangle) \\
 |\Psi\rangle_- &= \frac{1}{\sqrt{2}}(|01\rangle - |10\rangle) = \frac{1}{\sqrt{2}}(|HV\rangle - |VH\rangle) \\
 |\Phi\rangle_- &= \frac{1}{\sqrt{2}}(|00\rangle - |11\rangle) = \frac{1}{\sqrt{2}}(|HH\rangle - |VV\rangle)
 \end{aligned}$$

TABLE I: The Bell states

- 1) *Beam Splitter*: The beam splitter has 2 input ports and 2 output ports. Each input port is connected to the idler output from an SPDC process, and each output port is connected to the input port of a polarising beam splitter. One of the output ports, the reflected port, adds a  $180^\circ$  phase shift. Photons will both exit at any one port if they are indistinguishable; otherwise there is a 50:50 chance that they will either exit together through just one port or they will exit separate ports. The exit port(s) is a random selection.

As the SPDC process creates an H and V polarised pair of photons, any combination of H and V (HH, HV, VH, VV) can reach the beam splitter resulting in two scenarios when the photons are distinguishable (orthogonal polarisation) and two scenarios whereby they are indistinguishable.

Thus, statistically, in a perfect system, 50% of the time the photons will be indistinguishable and will transmit out a single port and a further 50% of the remaining photons will also transmit out a single port. Therefore, in an ideal system, 75% of the photons will transmit out a single port. Furthermore, the beam splitter may introduce a phase shift, which in the global setting can be ignored, thereby enabling the creation of states  $|\Phi\rangle_-$  and  $|\Psi\rangle_-$ .

- 2) *Hong–Ou–Mandel Visibility*: No system is ideal, and a major source of decoherence is introduced by the Hong–Ou–Mandel (HOM) visibility of the photons that interact in the beam splitter, see Hong et al. [11]. In the case of the ZALM source, the HOM visibility is concerned with how closely the two photons overlap spectrally, temporally, and in polarisation, with perfect overlapping in all three degrees of freedom producing completely indistinguishable photons. Anything less than perfect reduces the fidelity of the entanglement to the point that fidelity is zero if the photons are completely distinguishable.

- 3) *Polarising Beam Splitter*: The polarising beam splitter has a single input port<sup>2</sup>, which may receive 0, 1, or 2 photons, and two output ports which may emit 0, 1, or 2 photons depending on how many photons were received, and their polarisation. The output ports from the polarising beam splitters are each connected to a dedicated DWDM filter. The output at the polarising beam splitters determine which of the four Bell states the quantum system is in (but not its fidelity). See Fig. 3 for details.

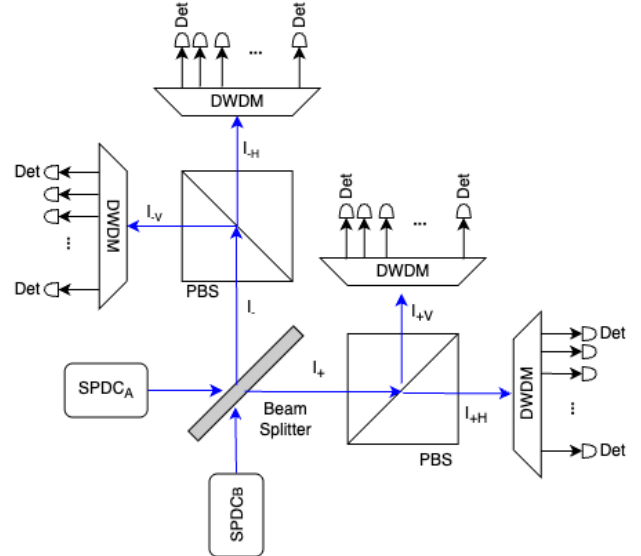


Fig. 3: Optical setup to determine which Bell state is detected.

If both photons are indistinguishable, they will exit the same port on both the beam splitter and the polarising beam splitter and will therefore create a  $|\Phi\rangle_+$  or  $|\Phi\rangle_-$  Bell state depending on whether they exited the  $I_+$  or  $I_-$  arm of the beam splitter. Photon Number Resolving detectors will be required to register the double click.

Otherwise, there is a 50% chance that the photons will both exit the same port of the beam splitter but different ports of the polarising beam splitter. In this scenario a  $|\Psi\rangle_+$  Bell state will be created as both photons will have the same phase.

In the final scenario, both photons will exit separate ports on the beam splitter, where one photon will exit the H arm of one of the polarising beam splitters and the second photon the V arm of the other polarising beam splitter. This will produce a  $|\Psi\rangle_-$  Bell state as there is a phase difference between

<sup>2</sup>Vacuum noise is not modelled in the PBS.

both photons. See Table I for a description of the polarisation encoded Bell states.

### C. DWDM Filtering and Detection

A DWDM filter is connected to each output of the polarising beam splitters. DWDM filters are assumed to have a detector per DWDM channel, regardless of channel bandwidth.

1) *DWDM Channels*: Four identical DWDM filters are used to determine the approximate wavelength of the idler photons. These DWDM filters will typically use a grid spacing slightly larger than the emitted photon bandwidth and the guardband bandwidth to provide the most accurate wavelength estimate. It is this specific feature that introduces the Zero-Added-Loss characteristics of ZALM.

2) *Heralding*: The detectors connected to the DWDM filters will determine which quantum state is expected based on the coincidence counts, see Fig. 3 for details. The detector click patterns, determined by phase and polarisation, and the central wavelength will be known. Any correcting information will be sent to the Post Processing unit and the timing and DWDM channel (wavelength) information will be sent to the receiver.

### D. Post Processing

Based on the Bell state detected, some operations may be applied the signal photons to transform them to the  $|\Psi\rangle^-$  state<sup>3</sup>. A fibre delay loop is placed between the signal port on the SPDC process and Pockels cells which are tuned to implement the Pauli gates necessary.

1) *Delay Line*: The processes within the ZALM source, from SPDC to heralding takes  $\sim 20$ ns. This equates to 4m of a fibre loop delay line. This is used to provide sufficient time to herald the idler photons, and enables the operations (gates) to be applied to the photons being emitted into the network.

2)  $|\Psi\rangle^-$  state (*singlet*): The singlet state is the preferred choice for the quantum memory, as it can be loaded with very high (unit) fidelity using the augmented Duan-Kimble protocol described by Raymer et al. [8].

Lastly, Shapiro et al. [10] provide a simple circuit that could be used to convert the polarisation encoded qubits into time-bin encoded qubits for more robust transmission over fibre.

## IV. IMPLEMENTATION / RESULTS

This ZALM source simulation is implemented in NetSquid, developed by Coopmans et al. [12], and uses the QSI Controller and APIs from Sekavčnik [13]. It can run standalone in NetSquid, or as part of a larger system within QSI.

The ZALM source is modelled on a table-top configuration where each component with conditional output paths is a distinct Node, i.e. the beam splitter is a separate node whereas the DWDM filters and the associated detectors are combined as the detectors have no output paths, rather they only register clicks. Each node has a quantum processor attached to it, which permits quantum operations (gates) to be applied to the

qubits. Quantum noise models are applied to these quantum processors, as described in Section IV-A. Furthermore, each node has a set of input and output ports, quantum channels, that are connected together via fibre of configurable length. Lastly, there is a classical information channel between the `HeraldingStation` and the `PostProcessors`.

A `NodeProtocol` runs on each node. The `NodeProtocol` is specific to the function of the node / component - such as; `BeamSplitterProtocol`, `FilterProtocol`, `PostProcessorProtocol`, etc. - and will execute a `QuantumProgram` when direct manipulation of qubits is required, i.e. `SPDCInitQubits`, `SPDCProgram`, etc. Signals are used to communicate between the `NodeProtocols`. These Signals act as triggers to other `NodeProtocols` and are used to pass monitoring / status information.

A `FlyingQubit` class, inherited from type `Qubit`, was created (`custom_qubits.py`) to add additional properties, frequency and polarisation, to the default `NetSquid` qubit. A density matrix formalism is used to represent the quantum states. All qubits are stored in the quantum memory associated with each node and are popped when an operation needs to be performed, including any gate or depolarising operations, and are then either placed back into memory or transmitted to the next port. The fibres between nodes have a fibre noise model applied.

A `utils.py` library provides supporting functions to the model, such as `calculate_visibility`, `determineBellState`, `generate_flex_dwdm_grid`, etc., `system_setup.py` builds and connects the node configuration into a network, and `config.py` stores the default configuration parameters described in Section IV-A. These parameters can be overridden in the config file or via the QSI API.

### A. Configuration options

The model can be run in either of two modes; `'IDEAL'` or `'REALISTIC'`. The `IDEAL` mode introduces no losses or noise sources into the model, which is useful for tracking the quantum states through the system, whereas the `REALISTIC` mode operates with standardised values from real-world components.

```
SIM_MODE 'REALISTIC'
          'IDEAL'
```

The default values for each configuration option in `REALISTIC` mode are now described.

The SPDC process has 6 configurable parameters which specify the pump laser wavelength (nm), the degeneracy bandwidth of the SPDC processes (nm), the jitter between both processes (ps), the output photon bandwidth (GHz), the probability of a successful SPDC emission, and the signal/idler separation method.

<code>SPDC_PUMP_WAVELENGTH_NM</code>	775.0
<code>SPDC_DEGENERACY_BANDWIDTH_FWHM_NM</code>	5.0
<code>TEMPORAL_JITTER_STDEV_PS</code>	20.0
<code>EMISSION_SUCCESS_PROBABILITY</code>	0.95
<code>PHOTON_FWHM_GHZ</code>	30.0
<code>SPDC_MODE</code>	'DICHROIC'
	'PBS'

<sup>3</sup>This action could be performed at the receiving side.

The Beam Splitter has 2 configurable parameters which specify the minimum HOM visibility to be determined indistinguishable and the insertion loss associated with it.

```
BEAMSPLITTER_HOM_THRESHOLD    0.99
BEAMSPLITTER_INSERTION_LOSS_DB 0.20
```

The Polarising Beam Splitter has 2 configurable parameters which specify the probability of a photon being emitted from the incorrect port and the insertion loss associated with it.

```
PBS_EXTINCTION_RATIO    0.001
PBS_INSERTION_LOSS_DB   0.20
```

The DWDM Filter has 6 configurable parameters which specify which DWDM bands are enabled, the DWDM grid bandwidth (GHz), the size of any guardbands, the insertion loss associated with it, and the filtering model in use.

```
ENABLED_BAND                [C, S, L]
GRID_GRANULARITY_GHZ        100
FILTER_PASSBAND_FRACTION    0.8
EFFECTIVE_FILTER_BANDWIDTH_GHZ 80
DWDM_FILTER_INSERTION_LOSS_DB 0.50
FILTER_MODEL                  'GAUSSIAN'
                              'BRICKWALL'
```

The Detectors have 2 configurable parameters, their detection efficiency and whether they are photon number resolving.

```
DETECTOR_EFFICIENCY    0.98
DETECTOR_TYPE           'STANDARD'
                       'PNR'
```

The QuantumProcessors have 4 configurable parameters, the gate error probability over a single gate, the gate error probability over two gates, the measurement dephasing probability, and the memory depolarization rate.

```
GATE_ERROR_PROB_SINGLE_QUBIT 1e-4
GATE_ERROR_PROB_TWO_QUBIT    1e-3
MEASUREMENT_DEPHASE_PROB     1e-3
MEMORY_DEPOLAR_RATE          1e3
```

The fibre INTERNODE\_LENGTH (km) is configurable between the heralding station and the measurement station to simulate a quantum channel.

```
INTERNODE_LENGTH 15
```

### B. Limitations

The pump laser is not modelled in the SPDC process. The EMISSION\_SUCCESS\_PROBABILITY configuration option is used to set the efficiency level. It should also be noted that this source does not provide an ebit rate per second, but rather per use. Additionally, if the non-degeneracy bandwidth is very narrow and a dichroic mirror configuration is in use, the DM\_INSERTION\_LOSS\_DB and DM\_CROSSTALK\_PROBABILITY should be increased to either reflect the higher losses near the boundary wavelength, or else swap the component to a WSS or DWDM filter by increasing the insertion loss and lowering the lower cross talk probability.

### C. Results

Fig. 4 demonstrates the configurability of the ZALM source model. It shows the average fidelity and number of emitted qubits at the source. Here we demonstrate an IDEAL system configuration, along with SPDC non-degeneracies of 1 nm and 5 nm, using dichroic mirrors or polarising beam splitters for idler separation, and standard or photon number resolving detectors. Whilst there is a reduction and some variation in the entanglement fidelity in comparison to the ideal source, there is a more pronounced impact on the ebit rate.

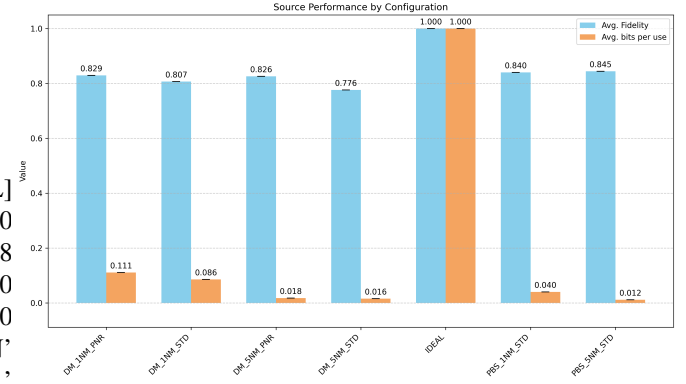


Fig. 4: Fidelity / Bits per use vs Configuration

Running the ZALM source in IDEAL mode and plotting the average fidelity and ebit rate vs distance, the initial fidelity is 1.0 which does not degrade over distance. However, the ebit rate drops inline with fibre losses, see Fig. 5. It should be noted that ZALM uses a source in the middle model configuration and therefore fibre distances are effectively doubled<sup>4</sup>.

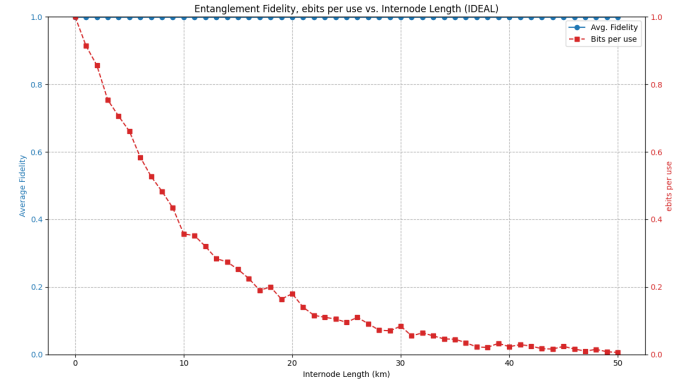


Fig. 5: Fidelity, ebits per use vs Distance, IDEAL setting

Using the default configuration parameters, the fidelity and ebit rate of the distributed entanglement is plotted against distance from 0 to 50 km, see Fig. 6.

It is clear that the ebit rate dramatically falls off, but the average fidelity remains high enough to be purified, which suggests that network performance will be limited by the latency of classical signaling for purification rather than the intrinsic quality of the raw entanglement.

Changing the SPDC\_DEGENERACY\_BANDWIDTH\_FWHM\_NM to 1.0 and the DETECTOR\_TYPE to PNR improves the ebit

<sup>4</sup>All fibre distances will be symmetric in the results shown.

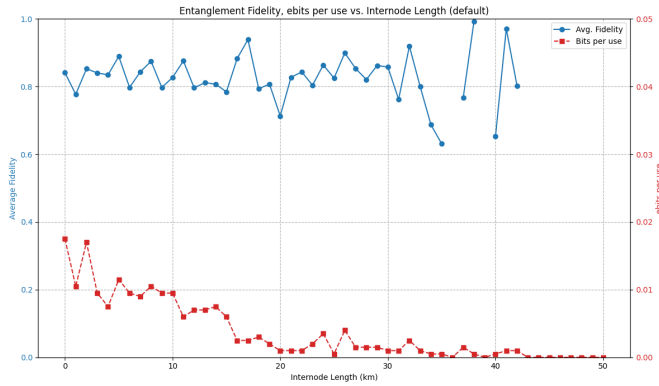


Fig. 6: Fidelity, ebits per use vs Distance, default settings

rate considerably, whilst the average fidelity remains roughly the same, see Fig. 7.

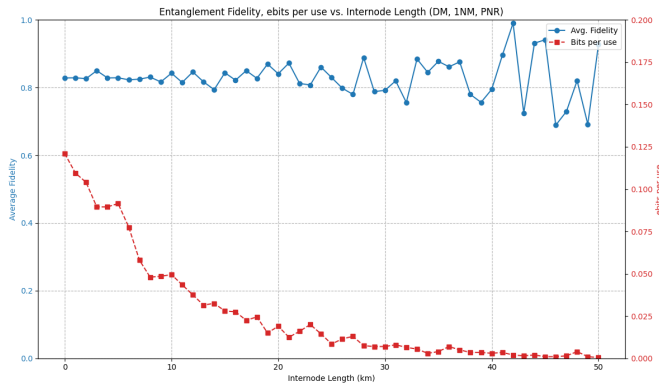


Fig. 7: Fidelity, ebits per use vs Distance, 1nm, PNR

## V. CONCLUSIONS

We have developed a modular simulation of a ZALM-type entanglement source. The model is highly configurable with over 20 key physical parameters that can be adjusted. Our simulation serves as a tool to co-design and optimise the source for maximal network efficiency. Furthermore, it provides a modular building block within the QSI library where larger quantum simulations can be created, allowing full end-to-end performance analysis of various component configurations to identify optimal operating modes for specific network architectures.

## REFERENCES

- [1] H. J. Kimble, “The quantum internet,” *Nature*, vol. 453, no. 7198, pp. 1023–1030, 2008.
- [2] S. Wehner, D. Elkouss, and R. Hanson, “Quantum internet: A vision for the road ahead,” *Science*, vol. 362, no. 6412, p. eaam9288, 2018.
- [3] M. D. Eisaman, J. Fan, A. Migdall, and S. V. Polyakov, “Invited review article: Single-photon sources and detectors,” *Review of scientific instruments*, vol. 82, no. 7, 2011.
- [4] R. Bali, A. N. Tittelbaugh, S. L. Jenkins, A. Agrawal, J. Horgan, M. Ruffini, D. C. Kilper, and B. A. Bash, “Routing and spectrum allocation in broadband quantum entanglement distribution,” *IEEE Journal on Selected Areas in Communications*, vol. 43, no. 5, pp. 1856–1870, 2025.
- [5] J. Weber, W. Koehl, J. Varley, A. Janotti, B. Buckley, C. Van de Walle, and D. D. Awschalom, “Quantum computing with defects,” *Proceedings of the National Academy of Sciences*, vol. 107, no. 19, pp. 8513–8518, 2010.
- [6] C. Bradac, W. Gao, J. Forneris, M. E. Trusheim, and I. Aharonovich, “Quantum nanophotonics with group iv defects in diamond,” *Nature communications*, vol. 10, no. 1, p. 5625, 2019.
- [7] E. Bersin, M. Sutula, Y. Q. Huan, A. Suleymanzade, D. R. Assumpcao, Y.-C. Wei, P.-J. Stas, C. M. Knaut, E. N. Knall, C. Langrock *et al.*, “Telecom networking with a diamond quantum memory,” *PRX Quantum*, vol. 5, no. 1, p. 010303, 2024.
- [8] M. G. Raymer, C. Embleton, and J. H. Shapiro, “The duan-kimble cavity-atom quantum memory loading scheme revisited,” *Phys. Rev. Appl.*, vol. 22, p. 044013, Oct 2024. [Online]. Available: <https://link.aps.org/doi/10.1103/PhysRevApplied.22.044013>
- [9] K. C. Chen, P. Dhara, M. Heuck, Y. Lee, W. Dai, S. Guha, and D. Englund, “Zero-added-loss entangled photon multiplexing for ground- and space-based quantum networks,” *Phys. Rev. Applied*, 2023.
- [10] J. H. Shapiro, M. G. Raymer, C. Embleton, F. N. Wong, and B. J. Smith, “Entanglement source and quantum memory analysis for zero-added-loss multiplexing,” *Physical Review Applied*, vol. 22, no. 4, p. 044014, 2024.
- [11] C. K. Hong, Z. Y. Ou, and L. Mandel, “Measurement of subpicosecond time intervals between two photons by interference,” *Phys. Rev. Lett.*, vol. 59, pp. 2044–2046, Nov 1987. [Online]. Available: <https://link.aps.org/doi/10.1103/PhysRevLett.59.2044>
- [12] T. Coopmans, R. Knegjens, A. Dahlberg, D. Maier, L. Nijsten, J. de Oliveira Filho, M. Papendrecht, J. Rabbie, F. Rozpedek, M. Skrzypczyk *et al.*, “Netsquid, a network simulator for quantum information using discrete events,” *Communications Physics*, vol. 4, no. 1, p. 164, 2021.
- [13] S. Sekavčnik, “QSI: A Quantum Simulation Interface for Interoperable Components,” October 2022, associated with the Special Issue on “Software for Quantum Networks” in *Advanced Quantum Technologies*. [Online]. Available: [https://github.com/tqsd/special\\_issue\\_quantum](https://github.com/tqsd/special_issue_quantum)